Improved Experimental Setup to Reach a Broad Frequency Domain in Local Electrochemical Impedance Spectroscopy Measurements

Maurilio Pereira Gomes, Samantha Michelle Gateman, Isolda Costa, Oumaïma Gharbi, Kieu Ngo, Jesualdo Luiz Rossi, Mireille Turmine, Vincent Vivier

Improved Experimental Setup to Reach a Broad Frequency Domain in Local Electrochemical Impedance Spectroscopy Measurements

Maurilio Pereira Gomes,[a,b] Samantha Michelle Gateman,[a,c] Isolda Costa,[b] Oumaïma Gharbi,[a,c] Kieu Ngo,[a,c] Jesualdo Luiz Rossi,[b] Mireille Turmine,[a,c] Vincent Vivier[a,c]

[(a)] Sorbonne Université, CNRS, Laboratoire Interfaces et Systèmes Electrochimiques (LISE), 4 Place Jussieu -75005 Paris, France

[(b)] Instituto de Pesquisas Energéticas e Nucleares, Centro de Ciência e Tecnologia de Materiais, Av. Prof. Lineu Prestes, 2242, Cidade Universitária, CEP 05508-000 São Paulo SP, Brasil

[(c)] Sorbonne Université, CNRS, Laboratoire de Réactivité de Surface (LRS), 4 Place Jussieu - 75005 Paris, France

Graphical abstract

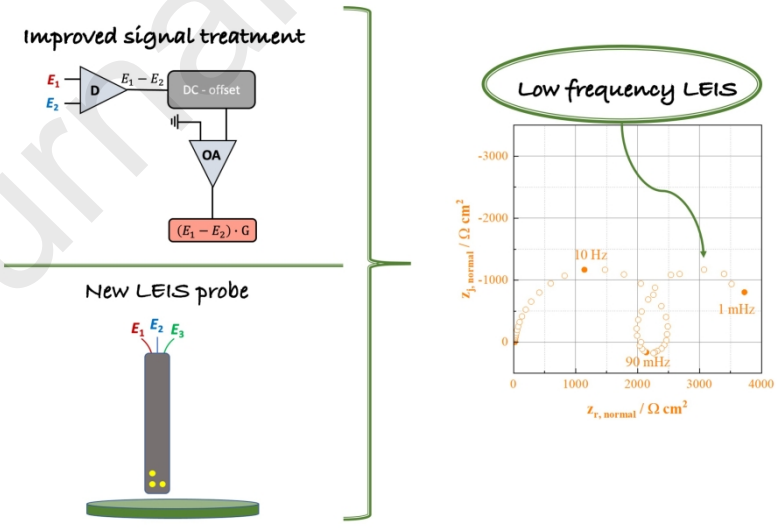

- A new LEIS setup is presented for performing low frequency measurements
- The development of local probes by soft lithography for sensing local current density allows broad-frequency measurements

- A comprehensive understanding of the local current densities is provided with the help of a newly developed equipment.

Abstract

We report a new experimental setup enabling local electrochemical impedance spectroscopy (LEIS) measurements over a wide frequency range, including the low frequency domain. First, an improved signal treatment was performed using a potential shifter to minimize the DC component of the measured potential, allowing for the local AC potential to be probed using an ideal electrochemical system. Then, a unique, three-electrode LEIS probe was implemented to study the influence of radial and lateral contributions on the LEIS response. The radial LEIS response is highest when the LEIS probe is positioned in the middle of the gold electrode substrate, whereas the lateral LEIS response is similar in both measured regions. Both experimental modifications were implemented to study the LEIS response over a corroding aluminum substrate, for which reliable results are obtained in the low frequencies. These tools could be used in future LEIS studies in other fields that require time-sensitive measurements.

Keywords: Scanning Electrochemical Probe Microscopy; Electrochemical Impedance Spectroscopy; Low frequency measurements; Electrochemical instrumentation; Micro-electrochemistry.

1. Introduction

The development of local electrochemical techniques such as scanning electrochemical microscopy (SECM) [1, 2], scanning vibrating electrode technique (SVET) [3], and scanning microcell [4] or scanning electrochemical cell microscopy (SECCM) [5], has enabled local reactivity measurements of various types of interfaces at different length scales. These techniques have been utilized to measure surface heterogeneity of interfaces including the solid electrolyte interphase formation on graphite [6], electrocatalytic materials [7], corroding metals [8], and bio-surfaces and interfaces [9].

Additionally, different approaches have been developed to take advantage of frequency-resolved local electrochemical techniques. For instance, the AC-mode of SECM has been devised using single frequency measurements for a fine control of the probe positioning [10, 11] and for imaging localized corrosion [12, 13]. However, AC-SECM relies on the EIS response of the microelectrode and how it is perturbed by the presence of the substrate, and does not directly measure the substrate's localized EIS response. The local electrochemical impedance spectroscopy (LEIS) technique was devised by Isaacs et al. [14, 15], taking advantage of local current density measurements using a bi-microelectrode (two stationary microelectrodes) as a local probe. The local potential difference between the two microelectrodes is then expressed as a local current density, j_{loc}, using Ohm's law and the geometric characteristic of the probe according to Eq 1:

$$j_{loc}(\omega) = \frac{\Delta E_{loc}(\omega) \cdot \kappa}{d} \qquad Eq.\ 1$$

where $\Delta E_{loc}(\omega)$ is the potential difference between the two microelectrodes at the frequency $f = \omega/2\pi$, κ is the bulk electrolyte conductivity, and d is the distance between the two microelectrodes. Using this local current density measured at different frequencies, it is possible to calculate the local impedance , z_{loc}, in Eq. 2 [16]:

$$z_{loc} = \frac{\Delta V_{ref}(\omega)}{j_{loc}(\omega)} \qquad Eq.\ 2$$

where $\Delta V_{ref}(\omega)$ is the applied potential perturbation at the substrate of interest with respect to the reference electrode.

An analysis of the various applications of LEIS reported in the literature shows that this technique can still be improved, both for high and low frequencies measurements [16, 17].

LEIS mapping is a technique that is often used to study degradation of protective coatings such as polymers for corrosion resistance [18, 19]. The main advantages of this technique for the corrosion and coating fields are that coating delamination can be locally measured (*i.e.*, detachment of the polymeric layer from the metal surface) prior to physical observation of lift-off, and it avoids the need to polarize the substrate far from its steady state. Such measurements are usually performed at a single frequency, most often chosen in the medium or high frequency range (*i.e.*, $f > 100$ Hz) and in low electrolyte concentration [20, 21], so that the duration of the experiment is short enough to assume a quasi-steady-state during the mapping and the AC potential measured at the bi-microelectrode is large enough to not be masked by the DC component of the potential.

To improve the spatial resolution of LEIS, both the size of each microelectrode and the inter-microelectrode distance must be reduced, thus resulting in a decrease in the measured AC potential difference. This reduction in AC potential difference poses the issue of the AC-potential contribution being masked by the large DC-current contribution, which stems from the electrochemical reactivity of the electrode material used to fabricate the bi-microelectrodes. The measurement of an AC-current contribution can be in the nA range or less (*i.e.*, potential differences in the range of the µV down to nV depending on the electrolyte conductivity), whereas the DC-current contribution may result in potential difference as high as few mV. Thus, the new device must first cancel the DC component before the amplification of the AC response of the system especially for the low frequencies. The solution of working in very dilute electrolytes usually proposed in the literature is however not acceptable because it corresponds to unconventional study environments. Moreover, decreasing the electrode size for improving spatial resolution generally results in a shortening the distance between the current collectors of each probe. This usually leads to a high-frequency stray-capacitance, which is added to the response and singularly complicates the interpretation in the high frequency domain.

The work presented herein aims to contribute to the LEIS community by providing methods on how to experimentally overcome these problems, that is, measuring LEIS in a broad frequency domain with a small electrode size in highly conductive media. The experimental measurement device developed for this work, namely the potential shifter and the tri-microelectrode LEIS probe, will be first presented and discussed. Then, a theoretical analysis of an electrochemical system will be investigated using finite element modeling. Finally, the proposed experimental solutions will be validated on two different experimental systems: the analysis of the electron

transfer on a model redox couple and the characterization of the corrosion of aluminum in acidic medium.

2. Experimental

The LEIS probes were manufactured by lithography. Briefly, a system of three gold microelectrodes was deposited on a thin glass slide using a standard lift-off process. This microfabrication method was chosen to control the size and the circular shape of each microelectrode, as well as move the wire current collectors away from each other to minimize the capacitive coupling that may exist when the two wires are too close together [22]. An example of a local probe fabricated for this work is shown in Figure 1a. It consisted of 3 gold micro-disk electrodes, each 50 µm in diameter, with a center-to-center distance of 100 µm. The current collectors are 50 µm wide and are covered with a thin SiO_2 insulating layer. Local probes from 10 to 100 µm have been fabricated using this protocol, but only results with 50 and 100 µm electrodes are presented in this article. The distance between the microelectrodes and the edge of the glass substrate was small in order to bring the device as close as possible to the surface of interest. From the local potential measurements made with these three microelectrodes, the calculation of the normal and radial components of LEIS can be carried out, as illustrated in Figure 1b. As already pointed out by numerous authors measuring local current density, the potential distribution in the electrochemical cell does not result in equipotential surfaces that are parallel to the electrode surface (except for specific electrode configurations). Thus, it is essential to measure these two contributions to accurately describe the local current density [16] since at a given location, the local current density can be calculated as the sum of local normal and local radial current density.

(a)

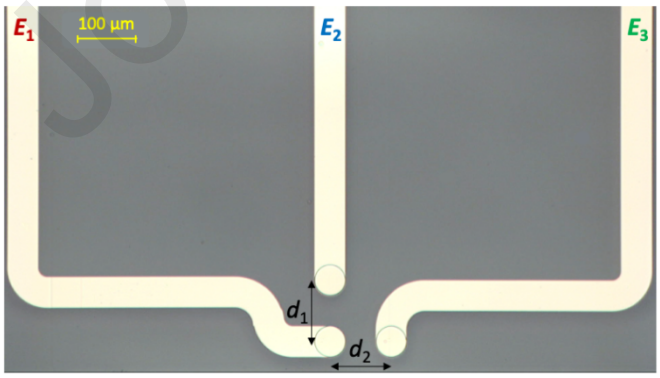

(b)

Normal local current density, j_{normal}

$$j_{normal} = \frac{(E_1 - E_2) \cdot \kappa}{d_1}$$

Radial local current density, j_{radial}

$$j_{radial} = \frac{(E_1 - E_3) \cdot \kappa}{d_2}$$

Figure 1: (a) Example of a three-electrode local probe for LEIS setup made by lithography – each electrode is 25 µm in radius and current collectors, which are covered by a thin insulating layer, are 50 µm wide – the active surface area for each electrode is delimited by the circle at the end of each strip; (b) definition of local current densities that can be measured with this probe.

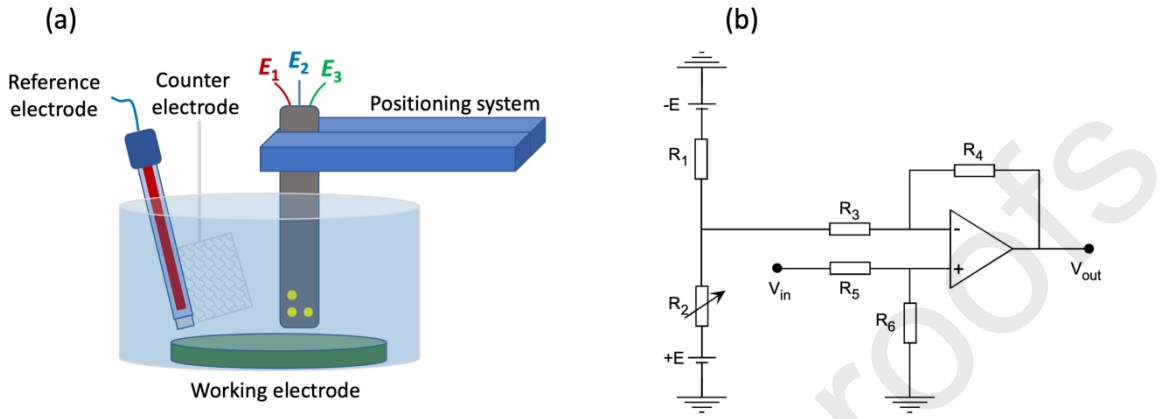

Figure 2: (a) Diagram of the experimental cell used to measure the local electrochemical impedance; (b) Circuit diagram of the potential shifter used in this work.

All electrochemical experiments were performed using a home-made LEIS setup sketched in Figure 2a and already described elsewhere [16], which consisted of a home-made potentiostat and a data acquisition card (National Instrument) controlled by an in-house developed software for the simultaneous measurement of multiple transfer functions. It provides the unique way of measuring simultaneously global and local EIS responses of the interface. The LEIS probe was positioned above the substrate with a 3-axis positioning system (M-VP- 25XA, Newport) driven by a motion encoder (ESP301, Newport) allowing a sub-micrometer spatial resolution in the three directions. Thus, in the present work, the probe dimension governs the attainable spatial resolution, which was in the range of a few micrometers depending on the probe size used and the distance to the substrate to analyze. Compared to the devices previously described in the literature, a specific amplification/offset device has been added to minimize the DC contribution of the potential difference between two microelectrodes Figure 2b. It consisted in a potential shifter inserted in the measuring circuit between the probes and the last amplification stage, allowing for the minimization of the DC potential contribution. During a preliminary measurement in the absence of any applied perturbation (*i.e.*, at the open circuit potential of the working electrode, when no impedance measurement is made), the potential difference measured at these microelectrodes is amplified by moderate gain, typically between 10 and 100 (which was shown to be a good range to allow a fine control of the potential with acceptable value for the common mode rejection ratio), and a potential shifter is added in the measurement

circuit to bring this DC potential difference as close as possible to 0 V. This allows small AC potential differences to be measured during impedance measurements using a higher gain since the analysis of the circuit shows an error of less than 1% for a potential difference of 1 mV at 1 Hz and this error increases with the frequency, but in that case, the AC-contribution (quantity of interest for the LEIS measurement) is also larger, making this circuit useful for the whole frequency domain. From an experimental point of view, it is worth noting that this device is also suited to circumvent the problem of measuring LEIS in concentrated electrolytes. As shown in Eq. 1, a high conductivity results in a low local current density measured. The electronic circuit depicted in Figure 2b enables the implementation of electrolytes with a similar conductivity to common electrochemical measurements, as it will be shown in the following with the experiments performed with ferricyanide/ferrocyanide redox couple.

As the local electrochemical impedance spectroscopy relies on the measurement of the local current density in solution arising from the potential gradient [3], it may be obtained by using local potential probes positioned close to the electrochemical interface. Similarly to the scanning vibrating electrode technique (SVET), two components of the local current density can be readily measured experimentally, namely the normal and the radial local current densities. In this work, the gold-deposited microelectrodes (Figure 1a) were used for measuring the normal local impedance, z_{normal}, as

$$z_{normal} = \frac{\Delta V_{ref}}{j_{normal}} = \frac{\Delta V_{ref} \cdot d_1}{(E_1 - E_2) \cdot \kappa} \qquad Eq.\ 3$$

and the radial local impedance, z_{radial}, as

$$z_{radial} = \frac{\Delta V_{ref}}{j_{radial}} = \frac{\Delta V_{ref} \cdot d_2}{(E_1 - E_3) \cdot \kappa} \qquad Eq.\ 4$$

where ΔV_{ref} is the applied perturbation potential between the reference and the working electrode, κ the electrolyte conductivity, E_1, E_2 and E_3 are the local potentials measured with the gold microelectrodes as depicted in Figure 1b, and d_1 and d_2 are the distances between the normal and the radial microelectrodes, respectively.

3. Numerical simulations

3.1. Model description

In this section, we present the main steps for performing the numerical simulations of both global and local LEIS taking into account the geometry of the electrochemical cell and the

current and potential distributions in the electrolyte. The detailed description can be found in previous works of different groups [23, 24]. For simplicity, we assume that the working electrode consisted in a planar disk-electrode embedded in an insulator. Such an assumption is in agreement with many experiments reported in the literature and allows the use of cylindrical coordinates for deriving the equations of the model. Let us consider a simple redox reaction in Eq 5:

$$Ox + ne^- \overset{k^0}{\leftrightarrow} Red \qquad Eq.\ 5$$

where k^0 is the kinetic constant of the electrochemical reaction, and n is the number of exchanged electrons. Assuming that the kinetics of this reaction follows the Butler-Volmer relationship, the total current at the working electrode, I, is given by Eq 6:

$$I = n\mathcal{F}Sk^0\left(C_{red}(0)\exp\left(\frac{\alpha n\mathcal{F}}{RT}(E-E^0)\right) - C_{ox}(0)\exp\left(\frac{-(1-\alpha)n\mathcal{F}}{RT}(E-E^0)\right)\right) \qquad Eq.\ 6$$

where $C_{red}(0)$ and $C_{ox}(0)$ are the concentrations of redox species at the interface, α is the charge transfer coefficient, E is the applied potential, E^0 is the formal redox potential, S is the electrode surface area, and the other parameters hold their usual meanings. Mass transport of electroactive species to the disk electrode is described by Fick's second law, which expresses k for each redox species, in cylindrical coordinate as

$$\frac{\partial C_k}{\partial t} = D_k\left(\frac{\partial^2 C_k}{\partial r^2} + \frac{1}{r}\frac{\partial C_k}{\partial r} + \frac{\partial^2 C_k}{\partial y^2}\right) \qquad Eq.\ 7$$

where D_k is the diffusion coefficient of the species k, r is the radial coordinate measured from the electrode center, and y is the normal coordinate to the electrode surface.

We thus followed the previous works of Gabrielli et al. [10] and Michel et al. [24] to calculate the faradaic contribution to the impedance at an inlaid disk-electrode using the finite difference method. We first assume that the EIS is performed at steady-state, thus the Fick's second law expresses as

$$\frac{\partial^2 C_k}{\partial r^2} + \frac{1}{r}\frac{\partial C_k}{\partial r} + \frac{\partial^2 C_k}{\partial y^2} = 0 \qquad Eq.\ 8$$

On the surrounding insulator, the flux of electroactive species is zero

$$\nabla C_k \cdot \boldsymbol{n} = 0 \qquad Eq.\ 9$$

where ∇C_k is the concentration gradient with respect to the r and y coordinates, and $\boldsymbol{n}$ is a unit vector normal to the boundary of the electrochemical system. Far from the electrode surface (i.e., in the bulk solution),

$$C_k \rightarrow C_k^* \text{ as } r^2 + y^2 \rightarrow \infty \qquad Eq.10$$

where C_k^* is the bulk concentration of the redox species k. At the electrode surface, the current can be split into a DC component and a harmonic component, where the latter is used to calculate the total impedance of the interface, obtained from the linearization of the Butler-Volmer relation [25].

Moreover, we also take into account the current and potential distributions due to the polarization and the geometry of the interface [25]. The potential, ϕ, in solution is governed by Laplace's relationship

$$\frac{\partial^2 \phi}{\partial r^2} + \frac{1 \partial \phi}{r \, \partial r} + \frac{\partial^2 \phi}{\partial y^2} = 0 \qquad Eq.\ 11$$

On the surrounding insulator and far from the electrode surface (i.e., on the counter electrode), the boundary conditions for solving the Laplace's law are expressed as

$$\left.\frac{\partial \phi}{\partial r}\right|_{y=0} = 0 \qquad Eq.\ 12$$

$$\phi \rightarrow 0 \text{ as } r^2 + y^2 \rightarrow \infty \qquad Eq.\ 13$$

whereas assuming an ideal capacitor (C_{dl}) for describing the double layer at the electrode interface, the current density at the electrode can be expressed as

$$i = C_{dl}\frac{\partial (E - E^0)}{\partial t} + n\mathcal{F}k^0\left(C_{red}(0)\exp\left(\frac{\alpha n\mathcal{F}}{RT}(E - E^0)\right) - C_{ox}(0)\exp\left(\frac{-(1-\alpha)n\mathcal{F}}{RT}(E - E^0)\right)\right) = \left.\frac{\partial \phi}{\partial r}\right|_{y=0} \qquad Eq.\ 14$$

This set of equations is then solved in the frequency domain, thus allowing the global impedance response of the electrode to be calculated together with the evaluation of the local impedance measured at various location in the electrolyte, above the surface of the working electrode.

3.2. Simulations

In this section, the simulation of the faradaic global and local EIS, taking into account potential distribution at different location above the electrochemical interfaces, are presented with the aim of positioning the problem and identifying the objectives to be achieved to improve the LEIS technique. Figure 3 shows the simulated global and local EIS responses accounting for a ferricyanide / ferrocyanide redox system in a supporting electrolyte. The simulations were performed assuming an electrolyte conductivity of 10 mS cm^{-1} (corresponding to a 0.5 mol L^{-1} NaCl solution), and 10 mmol L^{-1} for each electroactive species. The global impedance response presented in Figure 3a shows the usual features: electrolyte resistance as the high frequency limit of the impedance, a first capacitive time constant ascribed to the charge transfer resistance in parallel with the double layer capacitance, and a diffusion contribution in the low frequency domain corresponding to the Warburg impedance. The set of values used to carry out these simulations correspond to values usually encountered for a mono-electronic transfer involving soluble redox species. The resulting impedance diagram gives impedance values in the range of a few Ω to a few kΩ, i.e., values that can be easily measured with conventional equipment.

As expected for an ideal behavior for the working electrode, the LEIS response measured at 100 µm above the electrode center results in a similar shape to the global impedance response and the time constants observed remain unchanged as shown in Figure 3b-e. This is consistent with the fact that the processes probed locally are the same as those measured at the global scale. However, some differences exist and need to be discussed. The first point concerns the amplitude of the LEIS response. It depends on several parameters. The larger the distance of the local current measurement probe is, the smaller the potential difference to be measured and the greater the local current density. This results in large values of LEIS measured. The position of the probe above the working electrode is also a parameter to consider. Indeed, when it is close to the center of the working electrode (Figure 3b-c), the main contribution of the current is perpendicular to the surface of the electrode and results in a measured LEIS response obtained from the normal component of the local current density. In this case, the radial component can be neglected. On the other hand, when the probe is positioned above the edge of the working electrode (Figure 3d-e), the radial and normal components are of the same order of magnitude and neither can be neglected for the calculation of the LEIS response. It should be noted that current commercial devices only measure the radial component, thus limiting the possibility of qualitative analysis of the data obtained. It should also be mentioned that the low frequency limit of both local and global electrochemical impedances can significantly vary from one system the other. Actually, some systems may result in low magnitude impedance value in the

low frequency limit (*e.g.,* the iron dissolution in the active domain [26] or zinc dissolution [27]), whereas the impedance measured in the low frequency can be as high as a few MΩ up to a few GΩ (*e.g.,* passive films [28] or protective coatings on materials [29, 30]). For the latter, the potential difference to be measured in the low frequencies can be very small and requires the use of high gain amplification with a system similar to the one depicted in Figure 2b.

Another significant difference between local and global EIS responses (Figure 3) can be observed in the high frequency domain, which is in the frequency range where the electrolyte resistance is usually determined. The electrolyte resistance value depends on the tip-to-substrate distance; the larger the distance, the larger the uncompensated impedance and may exhibit some inductive and capacitive behavior due to the geometry of the system [31]. It was also shown that this frequency domain can be sensitive to the galvanic current that may exist, for instance, in the case of the corrosion of intermetallic particles embedded in a matrix [32, 33]. However, when small electrodes are used, such a behavior may be hindered by a stray capacitance that distorts the high frequency part of the impedance diagram [22], thus renders difficulty in conducting a proper analysis of this frequency domain.

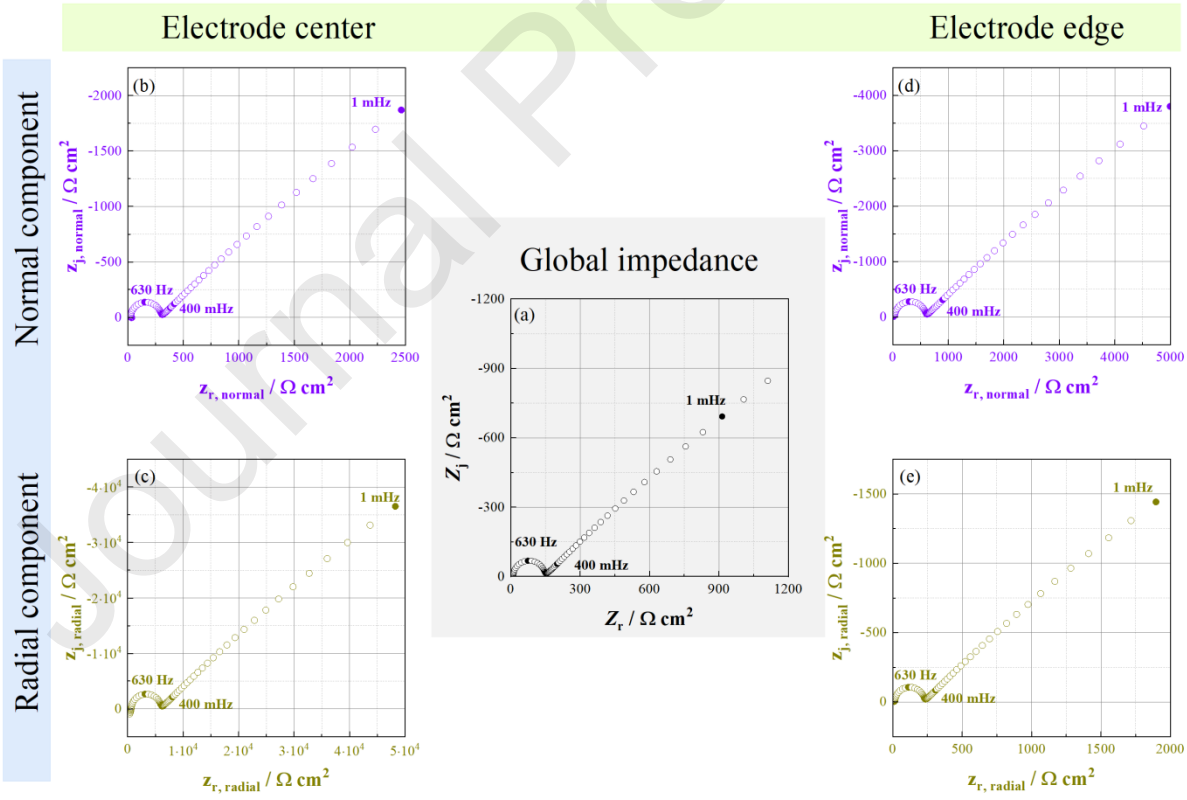

Figure 3: FEM simulation of the impedance response of an electrode immersed in Ox/Red solution (a), LEIS response at the electrode center - normal LEIS (b) and radial LEIS (c), and at the electrode edge - normal LEIS (d) and radial LEIS (e). Simulations were performed with $k^0 = 0.001$ *cm* s^{-1}, $\alpha = 0.5$, $E =$

E^0, $C^*_{ox} = C^*_{red} =$ 0.01 mol L^{-1}, $D_{ox} = D_{red} =$ 5 10^{-6} cm^2 s^{-1}, $C_{dl} =$ 10 μF cm^{-2}, $\rho =$ 100 Ω cm, $r_0 =$ 0.25 cm. LEIS spectrum were calculated at a distance of 100 µm above the electrode surface.

4. Results and discussion

4.1. Steady-state measurements

From the seminal work on the measurement of local current density that was later extended to the measurement of LEIS [16], the normal and the radial contributions to the LEIS response can be defined and measured experimentally [34]. Figure 4a shows the temporal potential evolution of the three local microelectrodes in a 0.5 M sulfuric acid solution measured against a mercury-mercurous sulfate electrode (MSE) reference. Even if these electrodes are identical, the DC potential measured slightly differs from one electrode to the other due to the different surface states of these microelectrodes. As a result, the potential difference between two microelectrodes is not zero as shown in Figure 4b. This quantity is added to the AC potential that we are interested in measuring. Indeed, if the potential difference that we want to measure is less than µV, the signal has to be amplified by at least a factor of ten thousand, which makes the measurement difficult due to amplification and resulting magnitude of the DC potential contribution measured simultaneously.

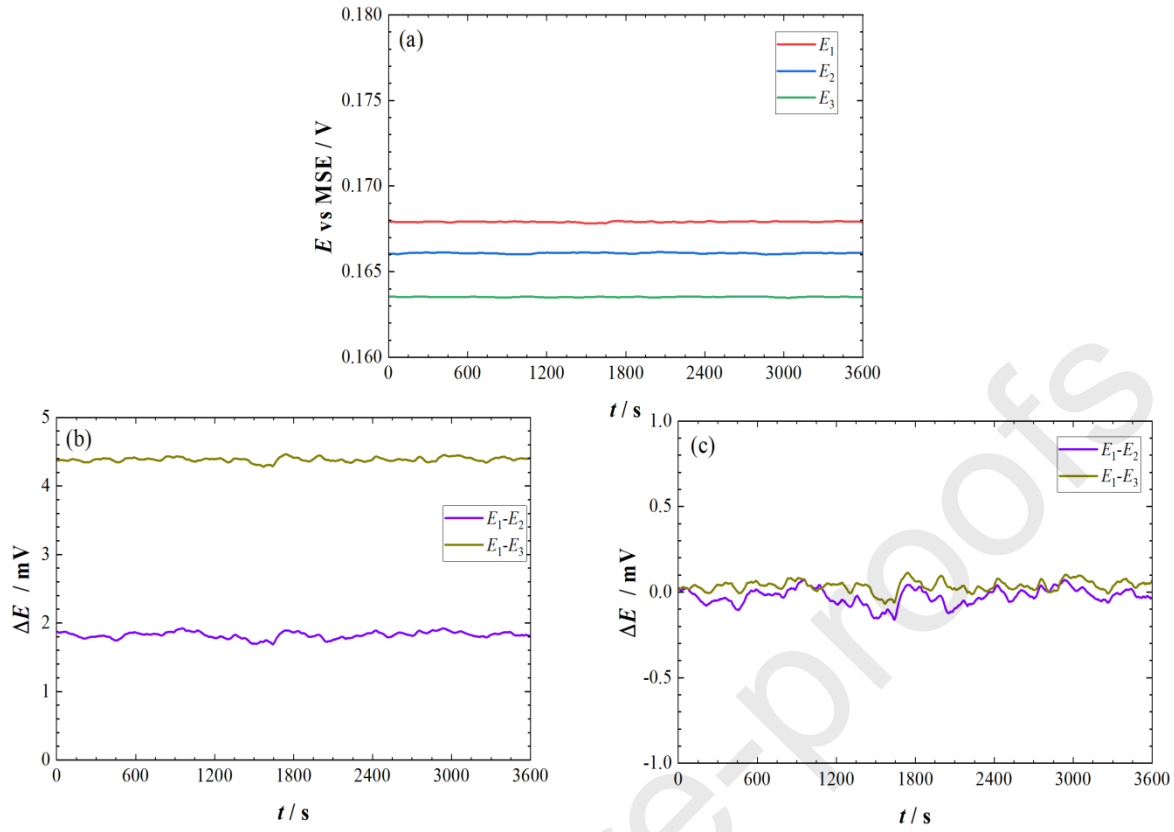

Figure 4: (a) Potential of the microelectrodes measured with respect to a MSE reference electrode for one hour in sulfuric acid solution; (b) potential difference between 2 microelectrodes before (b) and after (c) the DC – offset stage (see Figure 2b).

Conversely, if the measurement is performed following a two-step procedure, this problem is significantly minimized. The calibration step was added where the DC-potential difference is first amplified with a small gain (*e.g.*, 100 in the example presented in Figure 4c) then reduced to a value close to zero with an offset. This enables the measurement of the small AC potential using a high gain without having electronic overload problems. In the impedance measurements presented in the following work, this calibration step was used to measure large impedances and/or use concentrated solutions over a large frequency range.

4.2. Electrochemical impedance measurements

4.2.1. Impedance diagrams on redox soluble species

Figure 5 shows the global and local EIS diagrams measured simultaneously at the center of the gold electrode and at the edge of the electrode for the ferri/ferrocyanide system in 0.5 mol L^{-1} KCl electrolyte. These results should be directly compared to the simulations shown in Figure 3.

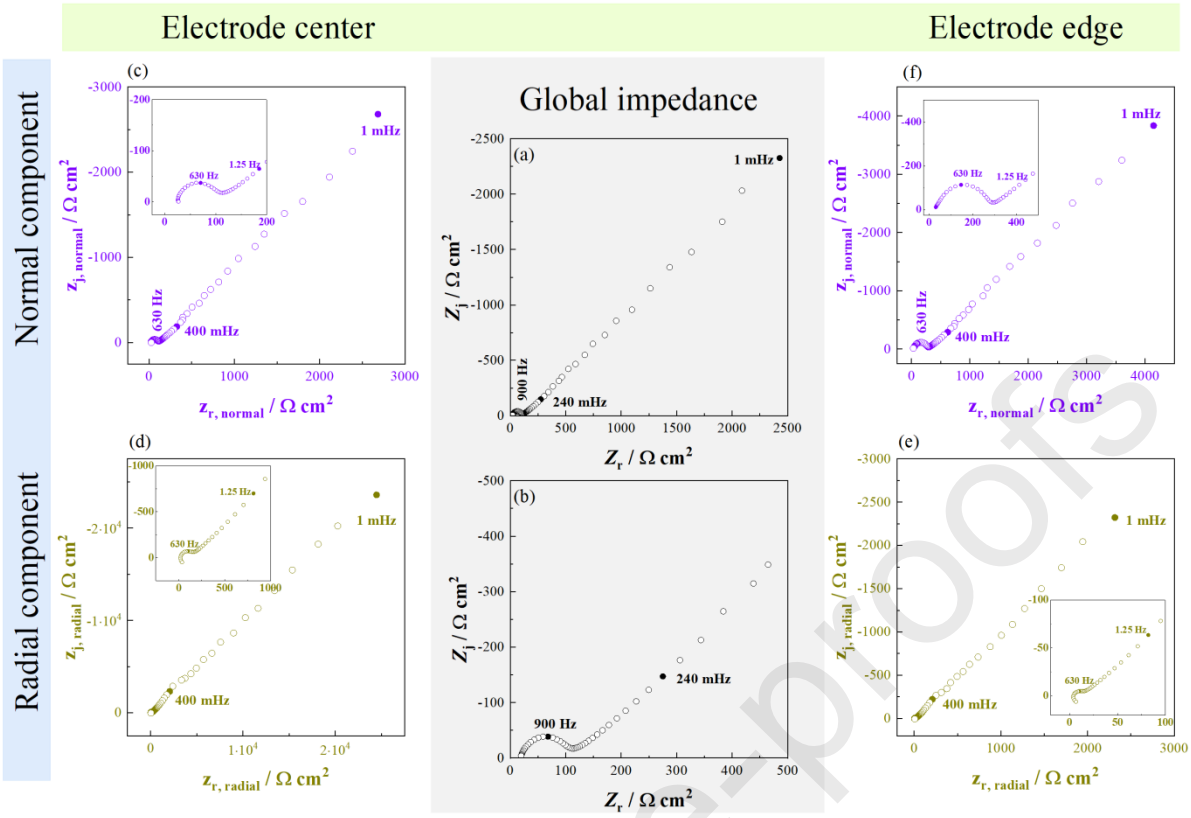

Figure 5: EIS and LEIS responses of ferri/ferrocyanide redox system at an Au electrode at the standard potential of the system (equimolar concentration of the electroactive species) in a 0.5 M KCl solution.

We observe the first time constant in the high frequency domain that corresponds to the charge transfer resistance in parallel with the double layer capacitance. In the medium to low frequency range, the Warburg diffusion is observed as a 45° line. These characteristics are identical to that obtained with local measurements, but with different amplitudes depending on whether the probe is positioned above the edge or the center of the working electrode, or whether the local current density measured corresponds to the radial or normal component. It should be noted that the mHz range can be measured, even for high impedance (greater than 2 10^4 Ω cm^2) in a concentrated solution. In the low frequency limit, one can also assume that the diffusion will be controlled by natural convection. In other words, the Warburg impedance describing semi-infinite diffusion may be not the correct way of describing the system, and a finite diffusion layer (*i.e.*, the Nernst diffusion layer) should be used. In that case, the characteristic frequency is the diffusion impedance, given by

$$f_c = 2.5\frac{D}{2\pi\delta_N^2} \qquad Eq.\ 5$$

where D is the diffusion coefficient of the electroactive species, and δ_N is the thickness of the Nernst diffusion layer. Assuming a diffusivity $D = 5 * 10^{-6}\,\mathrm{cm^2 s^{-1}}$ and a diffusion layer thickness $\delta_N = 300\ \mu\mathrm{m}$, a characteristic frequency of ca. 2 mHz is calculated, which is a value close to the low frequency limit used for performing experimental EIS and LEIS measurements. This result shows that the assumption of a semi-infinite Warburg diffusion remains valid in the whole frequency range investigated in this work.

In addition, the design of the probes with current collectors spaced far enough apart to minimize stray capacitance allows for evidence of ohmic impedance on LEIS diagrams at frequencies above 10 kHz as shown in the insets of Figure 5c-f.

4.2.2. Impedance diagrams on a corroding system

In order to show that this new experimental dispersive is suitable for any type of EIS measurement, the case of an aluminum electrode in sulfuric acid medium was studied Figure 6 and Figure 7. Even if the mechanism of dissolution of aluminum in acid medium is still a controversial subject, the objective in this study is not to study this mechanism, but rather to show that the LEIS allows the reactivity of materials to be characterized by several time constants.

Figure 6a shows the global EIS response of a pure Al electrode after one hour immersion in 0.5 mol L^{-1} sulfuric acid at the corrosion potential. Three time-constants can be clearly observed: in the high frequency domain, a capacitive loop can be ascribed to the charge transfer at the metal oxide interface in parallel with the capacitance of the thin oxide film [35, 36]. In the intermediate frequency domain, an inductive loop is observed, which usually is attributed to the relaxation of adsorbed ions such as oxygen anions that are present at the oxide/electrolyte interface [35, 37]. In the low frequency domain, the capacitive behavior can be ascribed either to the relaxation of adsorbate intermediates [35] or to the modulation of the thin oxide film thickness [38]. When LEIS measurements are performed above the working electrode center, the same response was obtained with three time-constants from both the normal (Figure 6b) and the radial (Figure 6c) local current density contributions. Interestingly, the characteristic frequencies remain unchanged and normal contribution is almost similar to the global EIS response. However, the amplitude of the inductive loop measured from the radial current density is larger, showing that this time-constant is sensitive to the position at which the measurements is performed. It is worth noting that despite the fact that the impedance value is

very high, it is possible with this new device to measure it. It is also noted that when the measurement is made at the center of the working electrode, the radial component is more than one hundred times higher, which indicates that this contribution is negligible.

Conversely, when the same measurement is performed on the edge of the electrode (Figure 7), the two components of the LEIS response are of the same order of magnitude. These results show two things: on the one hand it is possible to measure high LEIS at low frequency, and on the other hand, the radial component which is often presented for DC measurements [3] and often ignored for LEIS measurements, is an important contribution to the measured response, in particular when the probe is positioned near a discontinuity.

Local electrochemical impedance spectroscopy is also widely used for mapping the reactivity of an interface. For LEIS mapping, it is not common to perform measurements in the very low frequency domain since the acquisition of each point requires at least the equivalent time corresponding to one cycle of the applied perturbation. For example, at 10 mHz, the duration of the measurement is 100 s. For a picture of 100 by 100 points, this will require about 280 hours, i.e., more than 11 days. In fact, 1 Hz seems to be the limit for this particular application since it takes about 2.5 hours to acquire the entire image of the same size, assuming little or no change in the electrochemical system during this time.

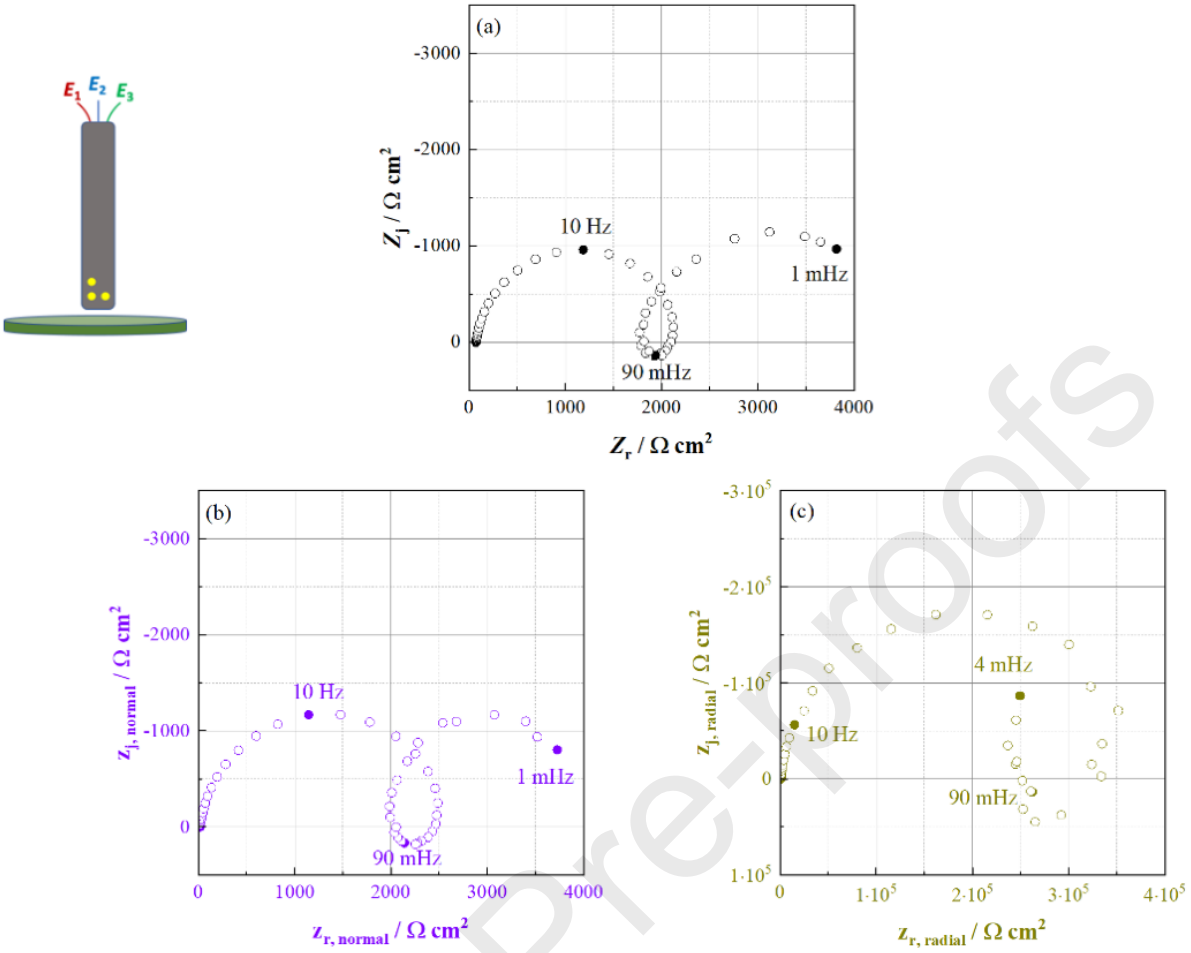

Figure 6: EIS responses of Al in 0.5 mol L^{-1} sulfuric acid solution at the corrosion potential – measured at the electrode center. (a) Global EIS, (b) normal component of the LEIS (c) radial component of the LEIS.

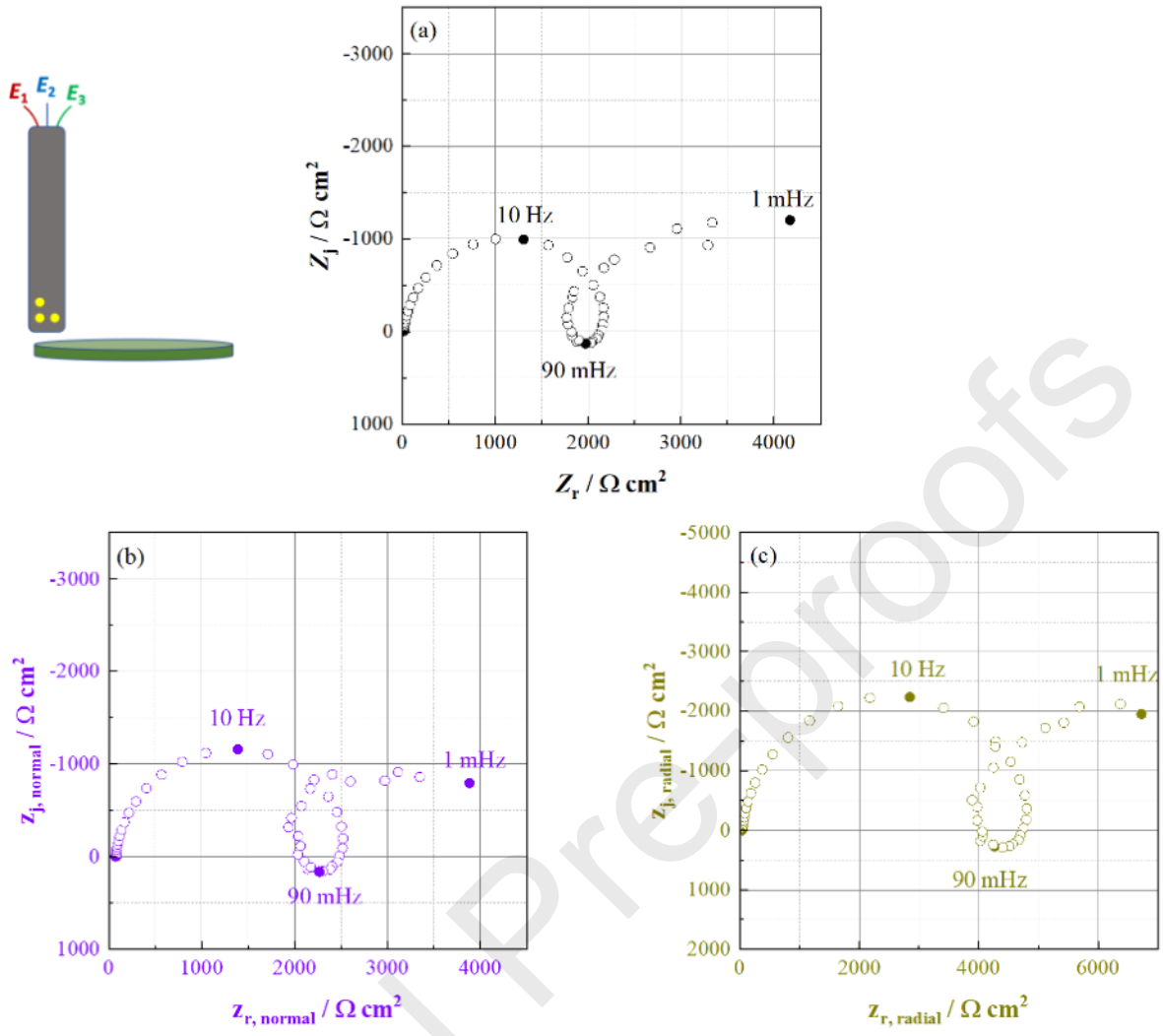

Figure 7: EIS responses of Al in 0.5 mol L^{-1} sulfuric acid solution at the corrosion potential – measured at the electrode edge. (a) Global EIS, (b) normal component of the LEIS, (c) radial component of the LEIS.

5. Conclusions

In the present work, we propose an improved measuring device to study the local electrochemical impedance spectroscopy of an interface. The improvement concerns two main points: the measurement device itself with the development of a local probe that allows us to eliminate the stray capacitance due to the coupling of the two gold tracks acting as current collectors to the microelectrodes; and the use of potential shifter to minimize the DC-potential offset between the microelectrodes. The latter is of particular interest since such an enhancement was shown to allow both measuring at low frequency (in the mHz range) and

working in concentrated electrolyte, as demonstrated with the experiments performed on the ferri/ferrocyanide redox couple as model system.

Acknowledgments

The authors acknowledge FAPESP (2013/13235-6) and CAPES-Cofecub (806-14) for the financial support to this research and also for the grant of Maurilio Pereira Gomes (88881.154406/2017-01).

List of symbols

C_k	Concentration of the species k - $k = ox$ or red (mol cm^{-3})
C_k^*	Bulk concentration of the species k- $k = ox$ or red (mol cm^{-3})
C_{dl}	Double layer capacitance (F cm^{-2})
d	Distance between two microprobes (cm)
D_k	Diffusion coefficient of the species k - $k = ox$ or red (cm^2 s^{-1})
E_{corr}	Corrosion potential (V)
E^0	Standard potential (V)
E_i	Local potential measured with the probe i (V)
$\mathcal{F}$	Faraday constant (96485 C mol^{-1})
f	Frequency (Hz)
f_c	Characteristic frequency (Hz)
I	Current (A)
i	Current density (A cm^{-2})
j_{loc}	Local current density (A cm^{-2})
j_{normal}	Local normal current density (A cm^{-2})
j_{radial}	Local radial current density (A cm^{-2})
k^0	Kinetic constant of the electrochemical reaction (cm s^{-1})
n	Number of exchanged electrons
R	Molar gas constant (8.314 J K^{-1} mol^{-1})
r	Radial coordinate measured from the electrode center (cm)
S	Surface area of the working electrode (cm^2)
T	Temperature (K)
t	Time (s)
y	Normal coordinate measured from the electrode surface (cm)

Z	Global impedance of the sample (Ω cm^2)
z_{loc}	Local impedance (Ω cm^2)
z_{normal}	Local normal impedance (Ω cm^2)
z_{radial}	Local radial impedance (Ω cm^2)
α	Charge transfer coefficient of the electrochemical reaction
ΔE_{loc}	Potential difference between two microprobes (V)
ΔV_{ref}	Potential difference between the substrate and the reference electrode (V)
δ_N	Thickness of the Nernst's layer
κ	Electrolyte conductivity (S cm^{-1})
ϕ	Potential (V)
ω	Angular frequency, $\omega = 2\pi f$ (rad s^{-1})

References

[1] T. Kai, C.G. Zoski, A.J. Bard, Scanning electrochemical microscopy at the nanometer level, Chem Commun (Camb), 54 (2018) 1934-1947.

[2] D. Polcari, P. Dauphin-Ducharme, J. Mauzeroll, Scanning Electrochemical Microscopy: A Comprehensive Review of Experimental Parameters from 1989 to 2015, Chem Rev, 116 (2016) 13234-13278.

[3] A.C. Bastos, M.C. Quevedo, O.V. Karavai, M.G.S. Ferreira, Review—On the Application of the Scanning Vibrating Electrode Technique (SVET) to Corrosion Research, J. Electrochem. Soc., 164 (2017) C973-C990.

[4] H. Krawiec, V. Vignal, R. Oltra, Use of the electrochemical microcell technique and the SVET for monitoring pitting corrosion at MnS inclusions, Electrochem. Commun., 6 (2004) 655-660.

[5] N. Ebejer, M. Schnippering, A.W. Colburn, M.A. Edwards, P.R. Unwin, Localized high resolution electrochemistry and multifunctional imaging: scanning electrochemical cell microscopy, Anal. Chem., 82 (2010) 9141-9145.

[6] D. Martín-Yerga, M. Kang, P.R. Unwin, Scanning Electrochemical Cell Microscopy in a Glovebox: Structure-Activity Correlations in the Early Stages of Solid-Electrolyte Interphase Formation on Graphite, ChemElectroChem, 8 (2021) 4240-4251.

[7] T. Bo, X. Wang, R. Jia, L. Han, H.L. Xin, H. Zhang, E.M. Miller, M.V. Mirkin, Probing Activities of Individual Catalytic Nanoflakes by Tunneling Mode of Scanning Electrochemical Microscopy, J. Phys. Chem. C, 125 (2021) 25525-25532.

[8] S.M. Gateman, I. Halimi, A.R. Costa Nascimento, R. Lacasse, R. Schulz, C. Moreau, R. Chromik, J. Mauzeroll, Using macro and micro electrochemical methods to understand the corrosion behavior of stainless steel thermal spray coatings, npj Materials Degradation, 3 (2019).

[9] Y. Zhou, Y. Takahashi, T. Fukuma, T. Matsue, Scanning electrochemical microscopy for biosurface imaging, Current Opinion in Electrochemistry, 29 (2021).

[10] C. Gabrielli, F. Huet, M. Keddam, P. Rousseau, V. Vivier, Scanning electrochemical microscopy imaging by means of high-frequency impedance measurements in feedback mode, Journal of Physical Chemistry B, 108 (2004) 11620-11626.

[11] M. Etienne, A. Schulte, W. Schuhmann, High resolution constant-distance mode alternating current scanning electrochemical microscopy (AC-SECM), Electrochem. Commun., 6 (2004) 288-293.

[12] C. Gabrielli, E. Ostermann, H. Perrot, V. Vivier, L. Beitone, C. Mace, Concentration mapping around copper microelectrodes studied by scanning electrochemical microscopy, Electrochem. Commun., 7 (2005) 962-968.

[13] K. Eckhard, W. Schuhmann, Alternating current techniques in scanning electrochemical microscopy (AC-SECM), Analyst, 133 (2008) 1486-1497.

[14] R.S. Lillard, P.J. Moran, H.S. Isaacs, A Novel Method for Generating Quantitative Local Electrochemical Impedance Spectroscopy, J. Electrochem. Soc., 139 (1992) 1007-1012.

[15] F. Zou, D. Thierry, H.S. Isaacs, A high-resolution probe for localized electrochemical impedance spectroscopy measurements, J. Electrochem. Soc., 144 (1997) 1957-1965.

[16] O. Gharbi, K. Ngo, M. Turmine, V. Vivier, Local electrochemical impedance spectroscopy: A window into heterogeneous interfaces, Current Opinion in Electrochemistry, 20 (2020) 1-7.

[17] L. Burczyk, K. Darowicki, Local electrochemical impedance spectroscopy in dynamic mode of galvanic coupling, Electrochim. Acta, 282 (2018) 304-310.

[18] Y. Ye, D. Zhang, T. Liu, Z. Liu, J. Pu, W. Liu, H. Zhao, X. Li, L. Wang, Superior corrosion resistance and self-healable epoxy coating pigmented with silanzied trianiline-intercalated graphene, Carbon, 142 (2019) 164-176.

[19] J.B. Jorcin, E. Aragon, C. Merlatti, N. Pebere, Delaminated areas beneath organic coating: A local electrochemical impedance approach, Corros. Sci., 48 (2006) 1779-1790.

[20] T. Thi Xuan Hang, T.A. Truc, T.H. Nam, V.K. Oanh, J.-B. Jorcin, N. Pébère, Corrosion protection of carbon steel by an epoxy resin containing organically modified clay, Surf. Coat. Tech., 201 (2007) 7408-7415.

[21] L. Cheng, H. Wu, J. Li, H. Zhao, L. Wang, Polydopamine modified ultrathin hydroxyapatite nanosheets for anti-corrosion reinforcement in polymeric coatings, Corros. Sci., 178 (2021).

[22] C.P.d. Abreu, C.M.d. Assis, P.H. Suegama, I. Costa, M. Keddam, H.G. de Melo, V. Vivier, Influence of probe size for local electrochemical impedance measurements, Electrochim. Acta, 233 (2017) 256-261.

[23] R. Ferrigno, H.H. Girault, Finite element simulation of electrochemical ac diffusional impedance. Application to recessed microdiscs, J. Electroanal. Chem., 492 (2000) 1-6.

[24] R. Michel, C. Montella, C. Verdier, J.P. Diard, Numerical computation of the Faradaic impedance of inlaid microdisk electrodes using a finite element method with anisotropic mesh adaptation, Electrochim. Acta, 55 (2010) 6263-6273.

[25] M.E. Orazem, B. Tribollet, Electrochemical Impedance Spectroscopy, Second ed., Wiley, Hoboken, New Jersey, 2017.

[26] M. Keddam, O.R. Mattos, H. Takenouti, Reaction model for iron dissolution studied by electrode impedance. I. Experimental results and reaction model, J. Electrochem. Soc., 128 (1981) 257-266.

[27] C. Cachet, F. Ganne, S. Joiret, G. Maurin, J. Petitjean, V. Vivier, R. Wiart, EIS investigation of zinc dissolution in aerated sulphate medium. Part II: zinc coatings, Electrochim. Acta, 47 (2002) 3409-3422.

[28] C.M. Abreu, M.J. Cristóbal, R. Losada, X.R. Nóvoa, G. Pena, M.C. Pérez, The effect of Ni in the electrochemical properties of oxide layers grown on stainless steels, Electrochim. Acta, 51 (2006) 2991-3000.

[29] A. Zomorodian, M.P. Garcia, T. Moura e Silva, J.C. Fernandes, M.H. Fernandes, M.F. Montemor, Corrosion resistance of a composite polymeric coating applied on biodegradable AZ31 magnesium alloy, Acta Biomater, 9 (2013) 8660-8670.

[30] B. Díaz, R. Figueroa, X.R. Nóvoa, C. Pérez, A. Pintos, The corrosion protection afforded by a commercial rust converter doped with graphene oxide, Electrochim. Acta, 342 (2020).

[31] I. Frateur, V.M.W. Huang, M.E. Orazem, N. Pebere, B. Tribolletd, V. Vivier, Local electrochemical impedance spectroscopy: Considerations about the cell geometry, Electrochim. Acta, 53 (2008) 7386-7395.

[32] L. Lacroix, C. Blanc, N. Pebere, G.E. Thompson, B. Tribollet, V. Vivier, Simulating the galvanic coupling between S-Al2CuMg phase particles and the matrix of 2024 aerospace aluminium alloy, Corros. Sci., 64 (2012) 213-221.

[33] J.B. Jorcin, H. Krawiec, N. Pebere, V. Vignal, Comparison of local electrochemical impedance measurements derived from bi-electrode and microcapillary techniques, Electrochim. Acta, 54 (2009) 5775-5781.

[34] J.V. Ferrari, H.G. De Melo, M. Keddam, M.E. Orazem, N. Pebere, B. Tribollet, V. Vivier, Influence of normal and radial contributions of local current density on local electrochemical impedance spectroscopy, Electrochim. Acta, 60 (2012) 244-252.

[35] J.H.W. deWit, H.J.W. Lenderink, Electrochemical Impedance Spectroscopy as a tool to obtain mechanistic information on the passive behaviour of aluminium, Electrochim. Acta, 41 (1996) 1111-1119.

[36] I.V. Aoki, M.C. Bernard, S.I.C. de Torresi, C. Deslouis, H.G. de Melo, S. Joiret, B. Tribollet, Ac-impedance and Raman spectroscopy study of the electrochemical behaviour of pure aluminium in citric acid media, Electrochim. Acta, 46 (2001) 1871-1878.

[37] T. Våland, K.E. Heusler, Reactions at the oxide-electrolyte interface of anodic oxide films on aluminum, J. Electroanal. Chem., 149 (1983) 71-82.

[38] H.J. de Wit, C. Wijenberg, C. Crevecoeur, Impedance Measurements during Anodization of Aluminum, J. Electrochem. Soc., 126 (1979) 779-785.

CRediT author statement

Maurilio Pereira Gomes: Investigation

Isolda Costa, Jesualdo Luiz Rossi, Oumaïma Gharbi: Writing- Reviewing and Editing

Samantha Michelle Gateman, Kieu Ngo, Mireille Turmine, Vincent Vivier:
Conceptualization, Methodology, Investigation, Writing- Reviewing and Editing

Laboratoire de Réactivité de Surface – UMR 7197 CNRS
4 place Jussieu – Casier 178 – 75252 Paris Cedex 05

Dr. Vincent Vivier
CNRS Senior Researcher

+33 (0)1 44 27 5521 (Office)
vincent.vivier@sorbonne-universite.fr